INTERNATIONAL JOURNAL OF AUTOMOTIVE AND MECHANICAL ENGINEERING
ISSN: 2229-8649 e-ISSN: 2180-1606
VOL. 21, ISSUE 3, 2024, 11554 – 11568
DOI: https://doi.org/10.15282/ijame.21.3.2024.8.0891

RESEARCH ARTICLE

Experimental and Numerical Modelling of Ballistic Impact on Fiber Metal Laminates Based on Aramid Fiber Reinforced Epoxy

M.S. Fadly[1]*, A. Purnowidodo[2], P.H. Setyarini[2], B. Bakri[1], S. Chandrabakty[1]

[1]Department of Mechanical Engineering, Faculty of Engineering, Tadulako University, Palu, Indonesia
[2]Department of Mechanical Engineering, Faculty of Engineering, Brawijaya University, Malang, Indonesia

ABSTRACT - This paper investigates the ballistic impact behavior of fiber metal laminates (FML) composed of aramid fiber-reinforced epoxy with a central layer of aluminum alloy Al5083. The research examines the ballistic performance influenced by factors such as hole shape and depth in the laminate and integrates both macro and microstructural analyses of FMLs. The FML variations studied included a perforated first layer with hole diameters of 3 mm and 5 mm, through which bullets penetrated. Ballistic tests were conducted from a firing distance of 5 meters using 9-mm cartridges loaded with full metal jacket bullets approximately 25 mm wide, fired at an angle perpendicular to the target surface. The experimental and simulation ballistic impact tests closely matched, with a 95.63% agreement and an error margin of about 4.37%. The FML resisted bullet impact by allowing perforation through three layers (the aluminum plate and the first and second aramid/epoxy plies) while forming a bulge due to longitudinal deformation in the final layer (the back plate). The experimental and simulation results showed similar trends, with a 5 mm diameter hole leading to a deeper bulge on the backside. Bullet penetration at the center, following a square pattern, resulted in the smallest bulge formation and a reduction in both initial and final bullet velocities. The fracture morphology indicates a ductile fracture, characterized by dominant dimple formations across the surface. The dimples in the FMLs are coarser than those in monolithic aluminum plates due to the reduced bullet velocity as it penetrates each layer of the target FMLs, significantly decreasing the remaining bullet velocity. In contrast, monolithic aluminum plates exhibit a minimal velocity decrease, resulting in smoother dimple fractures.

ARTICLE HISTORY
Received : 09th Feb. 2023
Revised : 23rd Jan. 2024
Accepted : 29th Aug. 2024
Published : 20th Sept. 2024

KEYWORDS
Ballistic impact
Fiber metal laminate
Perforated plate
Aramid fiber
Aluminum

1. INTRODUCTION

The military is at risk during defense and security operations on battlefields and hostile terrains, making bullet-resistant materials crucial. They provide an effective solution against medium to high-velocity bullets. The protective action of these systems is largely determined by their energy absorption and the ability to prevent penetration from impacts of bullets with different calibers. Bulletproof vests are categorized by the United States Department of Justice under the National Institute of Justice (NIJ) Standards 0101.04 and 0101.06, with classifications ranging from levels II-A, III-A, up to IV [3]. In modern times, bulletproof vests are made from synthetic fabrics and high-strength fibers such as aramid, spectra, twaron, or dyneema [4-6]. Bullet-resistant materials have been developed through the discovery of new materials, the integration of materials, and the manufacture of composites from metals, ceramics, and fiber-reinforced polymers. The aim is to reduce and absorb as much as possible the bullet's kinetic energy to stop its penetration [7-9]. The development of materials includes carbon nanotubes [10] and graphene [11]. Fiber Metal Laminates are extensively used in primary aircraft structural applications because they offer a lightweight design and superior mechanical properties compared to monolithic metal structures [12-14]. Composite materials are laminated, merging the high strength and stiffness of metals with their toughness and thermal properties, making FMLs highly effective [13,15-20].

Carrillo et al. carried out a low-velocity bullet impact ballistic test on polypropylene-reinforced aramid fiber FMLs. The results revealed that a 3/4-layer FMLs configuration offers excellent energy absorption potential. The specific strength versus absorbed energy curve indicated that FMLs have more load-carrying capacity compared to their constituent monolithic materials [21]. D.W. Lee et al. analyzed the behavior of FMLs using steel as a base material, with CFRP or GFRP, under low-velocity impact loads. The study concluded that the orientation of the fiber determines the direction of crack propagation on impact [22]. Finite element-based simulation techniques are also employed to explore bullet penetration through hard or challenging targets observed in empirical tests. Using the well-documented Ls-Dyna code, various bullet-resistant materials were successfully simulated for different threat levels [23-27]. Rashed et al. studied the ballistic response of a 12.7 mm projectile against a perforated structural steel plate, developing a finite element model to investigate the penetration process. The Johnson-Cook plasticity equation was applied in this analysis [28]. Nayak et al. used a material model based on orthotropic elasticity to develop finite element models that replicate projectile impact on aramid fabric composites [29]. These micromechanically-based numerical models provided input parameters to simulate the ballistic impact response using two primary approaches: the macro-homogeneous and meso-heterogeneous methods [30]. Mishra et al. conducted a series of experimental simulations to study the impact loads from ballistic attacks

*CORRESPONDING AUTHOR | M.S. Fadly | ✉ muhsyaifulfadly@gmail.com
© 2024 The Author(s). Published by Universiti Malaysia Pahang Al-Sultan Abdullah Publishing. This is an open access article under the CC BY-NC 4.0 International license

on steel plates with different hole sizes and shapes, revealing that the presence of holes suppresses the formation of adiabatic shear bands on monolithic plates [31].

Soft body armor typically utilizes a single layer of aramid fiber to provide protection against bullets up to Level III-A [3,4,32,33]. The impact of bullets causes the aramid fibers to deform inward, absorbing the kinetic energy of the bullets. This inward deformation, aligned with the bullet's trajectory, results in significant strain on the fibers until they eventually fail [34-36]. Aramid can be combined with other materials to produce layered composites with increased ballistic resistance. For instance, aluminum plates, known for their strength, impact resistance, and low density [37], can be combined with aramid/epoxy composites, which have a rugged structure, excellent vibration damping properties, and high resistance to dynamic loads [38,39]. These layered forms of FMLs can be developed as bullet-resistant materials. There are a limited number of papers that give facts about the dynamic behavior of FML made from epoxy-reinforced aramid fibers, and there is no research yet discussing hole patterns in materials with layered structures. This work reports research on the experimental and simulated ballistic impact response to FMLs made from aramid/epoxy fiber and aluminum alloy 5083. The effect of hole diameter and the bullet penetration position on perforated FMLs are observed.

2. EXPERIMENTAL METHODOLOGY

2.1 Materials

FMLs are constructed using a three-layer configuration, comprising two outer layers of 2 mm thick aluminum plate 5083 and a core made of four layers of aramid/epoxy. Aluminum plate 5083 and aramid fiber are cut to 150 x 150 mm size. The chemical composition of aluminum 5083 after testing optical emission spectroscopy (OES) is shown in Table 1. Aluminum plates in the first layer of FMLs are also made hollow with a middle of square center pattern, as shown in Figure 1.

Table 1. Chemical composition of Al5083

Composition (weight %)								
Al	Mg	Si	Fe	Cu	Mn	Cr	Zn	Ti
93.94	4.52	0.2	0.081	0.08	0.784	0.10	0.043	0.09
Ni	Pb	Re	Bi	Sn	V	Ca	Pr	
0.01	0.014	0.01	0.078	0.0087	0.0052	0.0005	0.04	

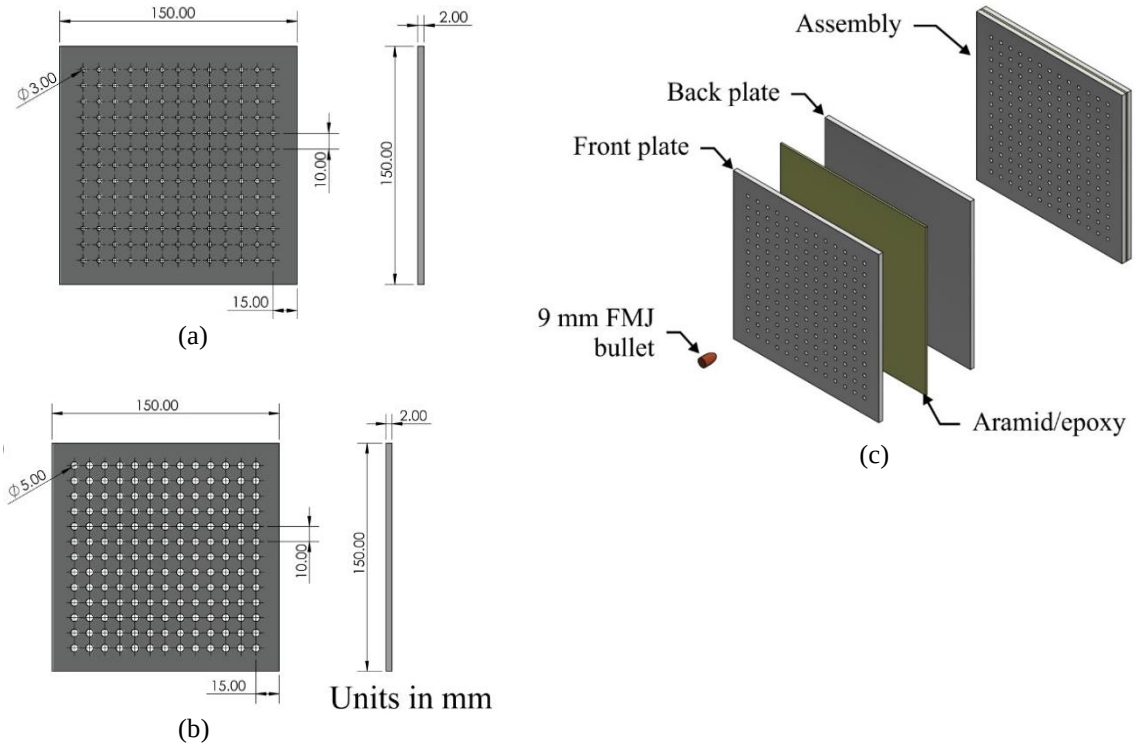

Figure 1. Dimensions and hole patterns: (a) 3 mm hole; (b) 5 mm hole; (c) fabricated FMLs with a hole

The specimens are prepared using vacuum-assisted resin infusion (VARI) methods (Fig. 2), where the resin and hardener mixture is drawn into the mold under vacuum pressure. FMLs utilize epoxy resins as their composite matrices. Aramid fiber, a class of heat-resistant and strong synthetic fibers derived from aromatic polyamide (aramids), specifically paraphenylene terephthalamide, features amides and benzene rings in its polymer chain. The high modulus and tenacity

of the fiber are due to strong inter-chain bonding and crystallinity [40]. Aramid fiber exhibits tensile strengths ranging from 2400 to 3600 N/mm² with elongation percentages of 2.2% to 4.4%. The tensile modulus of these fibers is between 60 and 120 GPa [41]. The basic mechanical properties of epoxy resin, as reported by Maples et al., include a density of 1.2–1.4 g/cm³, a tensile modulus of 2.5–5.0 GPa, and tensile strengths up to around 50–110 MPa [42]. When the hardener breaks the C–O–C rings, the epoxy resin polymerizes, forming a three-dimensional network of crosslinked molecules [43].

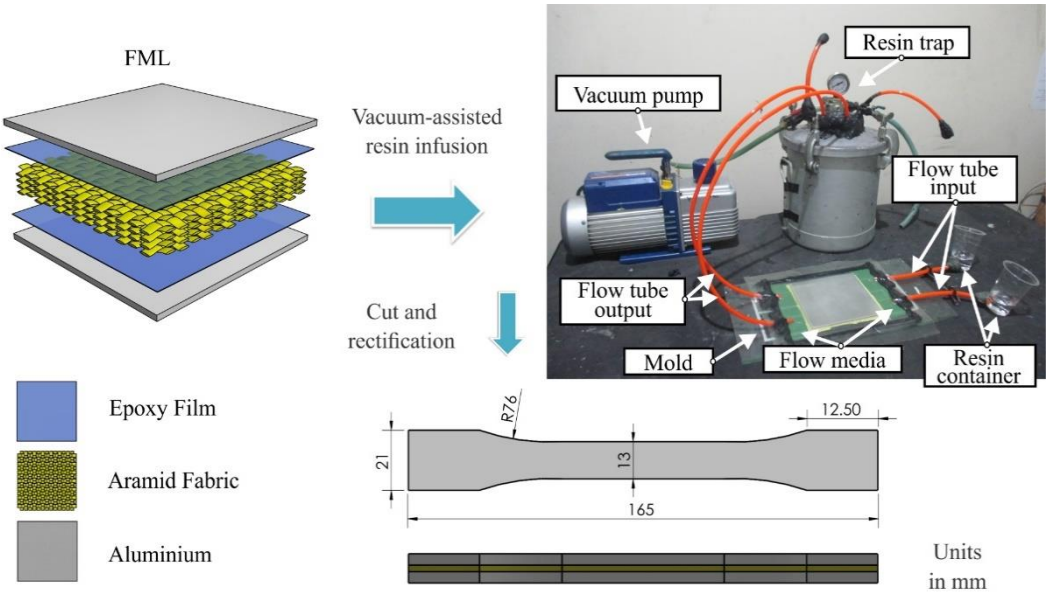

Figure 2. Stacking sequence of the FML and specimen for tensile testing

2.1.1 Tensile properties of the FMLs and the constituent materials

The properties of FMLs and their components are evaluated through tensile testing in accordance with ASTM D-638-03, as illustrated in Figure 2. This testing is conducted using the Universal Testing Machine (UTM) TN 20 MD control lab with a capacity of 200 KN. The results from these tensile tests are also utilized as references for material modeling in simulations.

2.2 Ballistic Test

The experimental ballistic test is conducted in accordance with the National Institute of Justice (NIJ) Standard 0101.06 Level III-A [3]. A 9 mm full metal jacket (FMJ) bullet with a hemispherical tip is fired using a Metrillo pistol. The setup for the ballistic test is displayed in Figure 3.

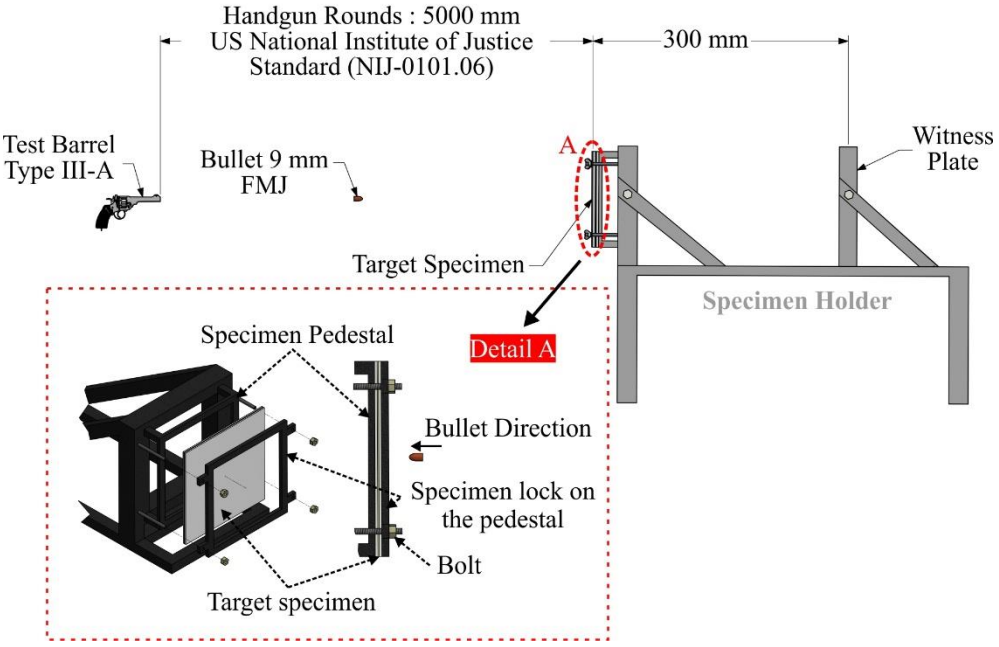

Figure 3. The ballistic testing scheme in accordance NIJ Standard 0101.06 level III-A

2.3 Numerical Models

Finite element-based simulations (explicit dynamics) are performed using Ansys 18.1 workbench software. The geometry of bullets and FML models are similar to those of experimental testing. The property scores of each material are input into the engineering data. The elastic material model is assumed to be linear with respect to the modulus of elasticity and Poisson's ratio. The finite element analysis uses an elastic-plastic material model with the Johnson-Cook metal failure criteria in the simulation. Both the bullets and aluminum plates are described using Johnson-Cook plasticity, as shown in Equation 1 [44]:

$$\sigma_{eq} = (A + B\,\varepsilon^{n}) \left(1 + C\,ln\,\frac{\dot{\varepsilon}}{\varepsilon_{o}}\right) \left(1 - \left(\frac{T-Tr}{Tm-Tr}\right)^{m}\right) \tag{1}$$

where σ_{eq} represents the equivalent stress, A denotes the yield stress constant, B signifies the hardening constant, ε stands for the equivalent strain, C indicates the strain rate constant, n is the hardening exponent, m is the thermal softening exponent, $\dot{\varepsilon}$ is the strain rate test, εo is the reference strain rate, T is the test temperature (K), Tr is the room temperature (K), and Tm is the melting temperature of the material (K). The Johnson-Cook damage model predicts the material failure criteria, determining the equivalent strain (ε_{pl}) at the onset of damage, as described in Equation 2 [8]:

$$\varepsilon^{pl} = \left[d_1 + d_2\,exp\left(d_3\,\frac{p}{q}\right)\right]\left[1 + d_4\,ln\left(\frac{\dot{\varepsilon}^{pl}}{\dot{\varepsilon_o}}\right)\right] \tag{2}$$

where ε^{pl} is the equivalent plastic strain, d1–d4 are material parameters, P represents the pressure stress, q denotes the Mises stress, and ε^{pl} indicates the plastic strain rate, with $\dot{\varepsilon_o}$ as the reference strain rate. The aramid/epoxy material is modeled using an orthotropic material model. If the material exhibits three perpendicular planes of symmetry, the rigidity matrix is indicated as shown in Equation 3 [45] and its stress-strain relationship is shown with inverse matrix [C_{ij}], so it becomes [S_{ij}] as shown in Equation 4 [46].

$$\begin{bmatrix}\sigma_1\\ \sigma_2\\ \sigma_3\\ \tau_{23}\\ \tau_{31}\\ \tau_{12}\end{bmatrix} = \begin{bmatrix}C_{11} & C_{12} & C_{13} & 0 & 0 & 0\\ C_{21} & C22 & C_{23} & 0 & 0 & 0\\ C_{31} & C_{32} & C_{33} & 0 & 0 & 0\\ 0 & 0 & 0 & C_{44} & 0 & 0\\ 0 & 0 & 0 & 0 & C_{55} & 0\\ 0 & 0 & 0 & 0 & 0 & C_{66}\end{bmatrix}\begin{bmatrix}\varepsilon_1\\ \varepsilon_2\\ \varepsilon_3\\ \gamma_{23}\\ \gamma_{31}\\ \gamma_{12}\end{bmatrix} \tag{3}$$

$$[S_{ij}] = \begin{bmatrix} \frac{1}{E_1} & -\frac{v_{21}}{E_2} & -\frac{v_{31}}{E_3} & 0 & 0 & 0\\ -\frac{v_{12}}{E_1} & \frac{1}{E_2} & -\frac{v_{32}}{E_3} & 0 & 0 & 0\\ -\frac{v_{13}}{E_1} & -\frac{v_{23}}{E_2} & \frac{1}{E_3} & 0 & 0 & 0\\ 0 & 0 & 0 & \frac{1}{G_{23}} & 0 & 0\\ 0 & 0 & 0 & 0 & \frac{1}{G_{31}} & 0\\ 0 & 0 & 0 & 0 & 0 & \frac{1}{G_{12}} \end{bmatrix} \tag{4}$$

2.4 Meshing Element

Meshing divides the model being considered into smaller areas. The purpose of meshing selection is to determine the desired precision level for simulation results. Before establishing the numerical study, mesh convergence was performed to verify the accuracy of the grid. For all FMLs, five mesh sizes ranging from 0.9 mm to 2 mm were chosen and analyzed. Figure 4 presents the mesh comparison of these FMLs under ballistic impact, showing bullet velocity reduction and force reaction target. An element size of less than 1.2 mm was found to converge the residual velocity and force response, as shown in the figure. The results for the mesh size of 0.9 mm are surprisingly close to each other, considering the depth of penetration (DOP). Therefore, meshing is done on FMLs with 0,9 mm in size and tetrahedron-shaped meshing. The results of meshing on FMLs and bullets are shown in Figure 5.

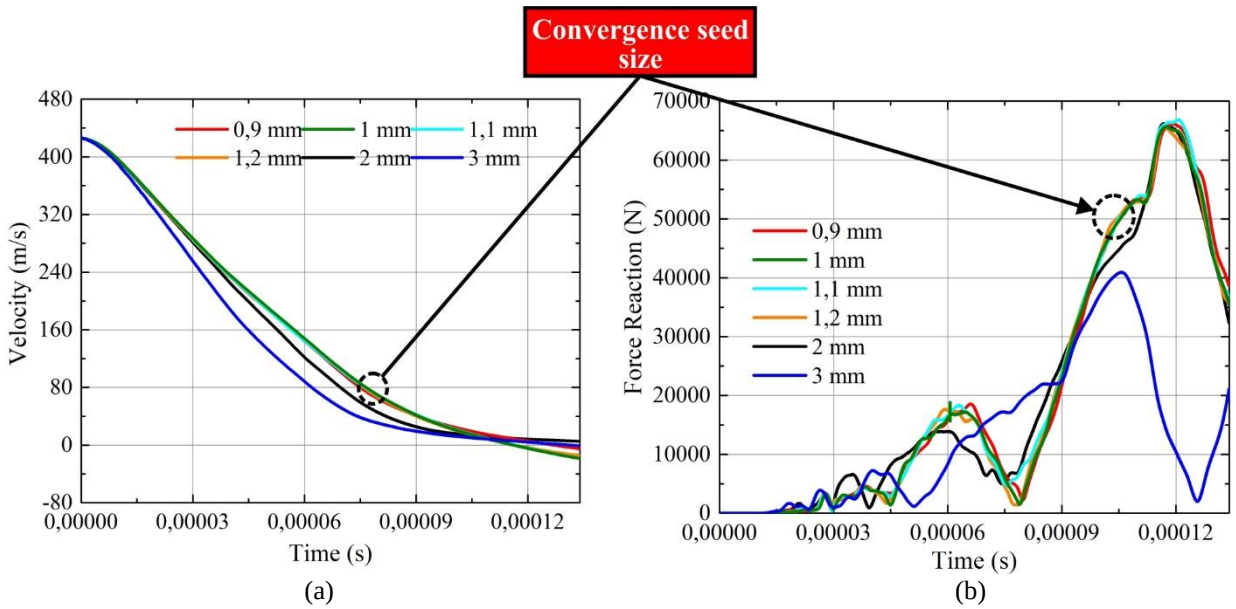

Figure 4. Numerical mesh convergence tests for seed 0.9, 1, 1.1, 1.2, 2 and 3 mm: (a) velocity reduction, (b) force reaction

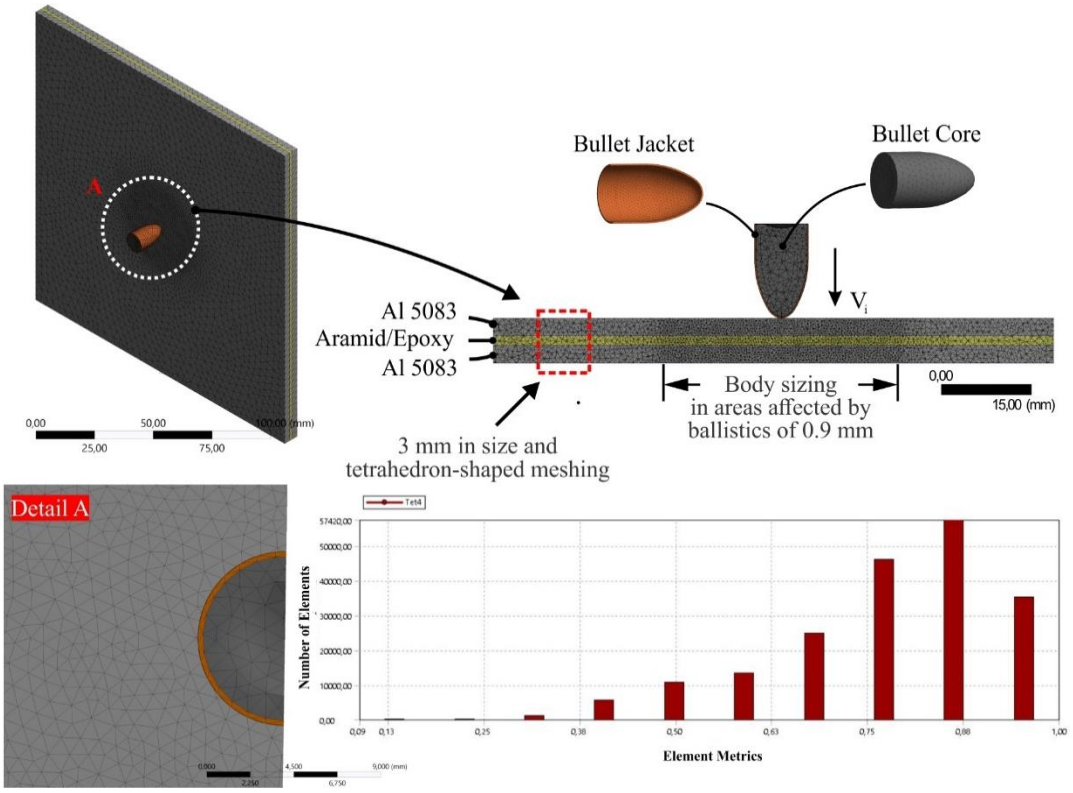

Figure 5. Meshing FMLs

3. RESULTS

3.1 Tensile Testing of the FMLs and Individual Components

A stress-strain curve of Al5083, composites, and FMLs after tensile testing is depicted in Figure 6. This shows that the highest strength among the constituent materials of FMLs is found in composites, followed by FMLs and then aluminum. The composite has the highest tensile strength of 410.72 MPa and the lowest strain value of 4.71%. Al5083 has the lowest strength at 212.78 MPa with a strain of 9.92%, while FMLs have a tensile strength of 330.11 MPa and a strain of 5.96%. The tensile properties of these materials, derived from the engineering stress-strain curves, are presented in Table 2.

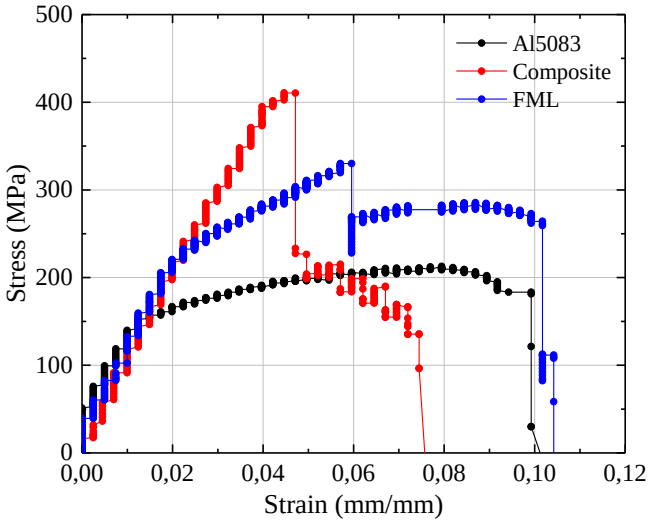

Figure 6. Stress-strain curve for aluminum, aramid/epoxy composite, and FML

Table 2. Tensile characteristics of FMLs and their component materials

Material	Young's modulus (MPa)	Yield strength (MPa)	Ultimate Tensile strength (MPa)	Strain at UTS (mm/mm)
Al5083	70.35	164.38	212.78	0.081
Composite	20.06	-	410.40	0.047
FML	48.94	108.13	330.11	0.059

Validation of numerical simulations was carried out using numerical simulations and test results, as shown in Figure 7. The depth of penetration of ballistic impacts on numerical simulations and experiments is measured. The measurement results show that the level of ballistic impact similarity is 95.63% or with an error percentage of 4.37%.

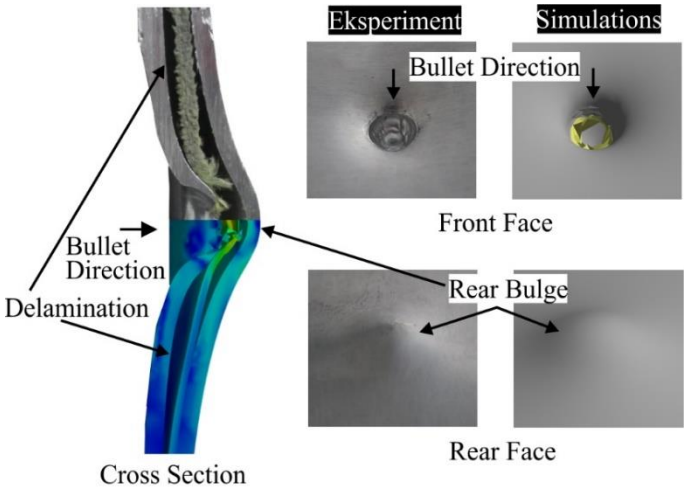

Figure 7. Ballistic test result

3.2 Ballistic Test

3.2.1 Constituent materials

Figure 8 shows the ballistic impact of the Al5083 plate due to bullet penetration. Deformation formed on the bullet impact area and moved away from the impact area. The hole characteristic of the Al5083 plate occurred as fractures around the edge of the hole on the backside. On the front side, it can be seen that the diameter of the hole was pushed forward in the direction of the bullet, while on the back side, it looked like petals. The formation of fractures, such as petals, and deformation on the backside show that the plate is both ductile and soft, which causes bullets to perforate the material along with plastic deformation. This is consistent with the statement of Iqbal et al. that the ductile material affected by the bullet will experience petaling failure [47]. The distribution and concentration of stresses on the Al5083 plate are shown in Figure 9.

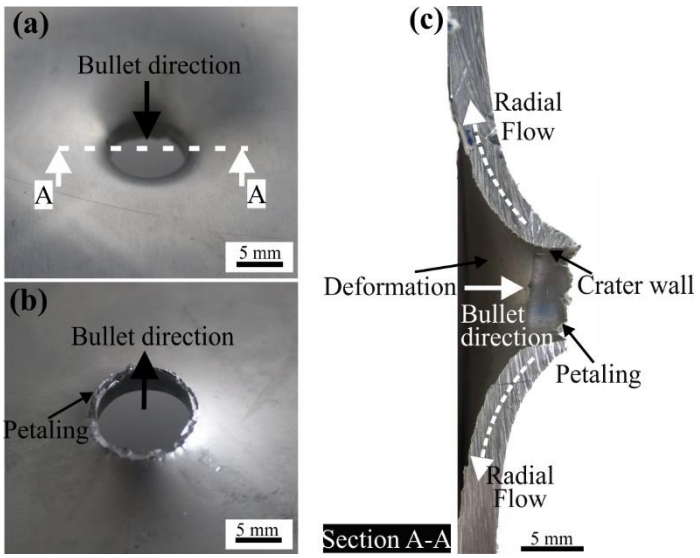

Figure 8. Ballistic impact in the aluminum

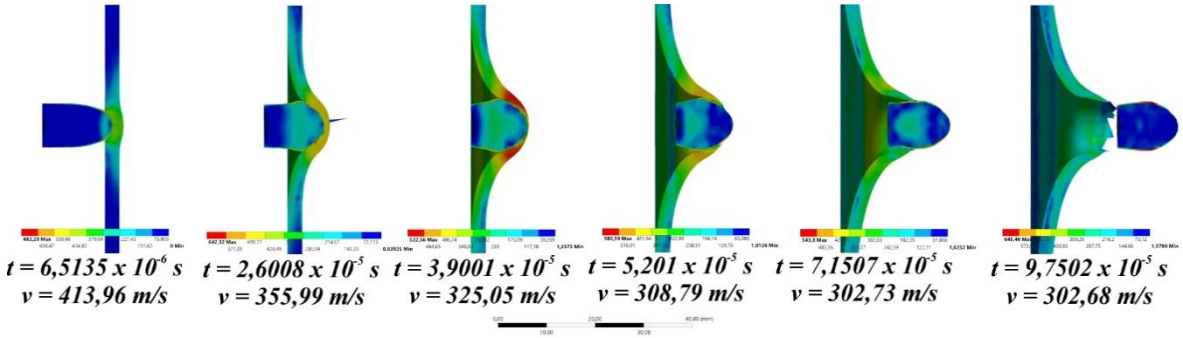

Figure 9. Impact process of the bullet on aluminum configuration (equivalent stress-von misses)

The stress concentrations occurring in bullets and plates in the impact zone resulted in deformation where the velocity, which was initially 426 m/s, decreased to 413.96 m/s. In the next second, that is 2.6008 x 10-5, showed that the plate started to deform in the direction of the bullet and reached the maximum stress value spread in the area of the bullet impact zone, reaching 522.56 MPa at 3.9001 x 10-5 seconds with a bullet velocity of 325.05 m/s. Al monolithic plate was unable to hold the bullet, so the plate was perforated at 5.201 x 10-5 seconds. The maximum stress that occurred on a plate is shown in red, while the core of the bullet (lead) low-stress distribution that occurred is indicated in blue. This caused the bullet penetration into the Al monolithic plate to deepen, eventually perforating the plate. The macroscopic characteristic of aramid/epoxy due to ballistic impact from 9 mm FMJ caliber bullets is shown in Figure 10.

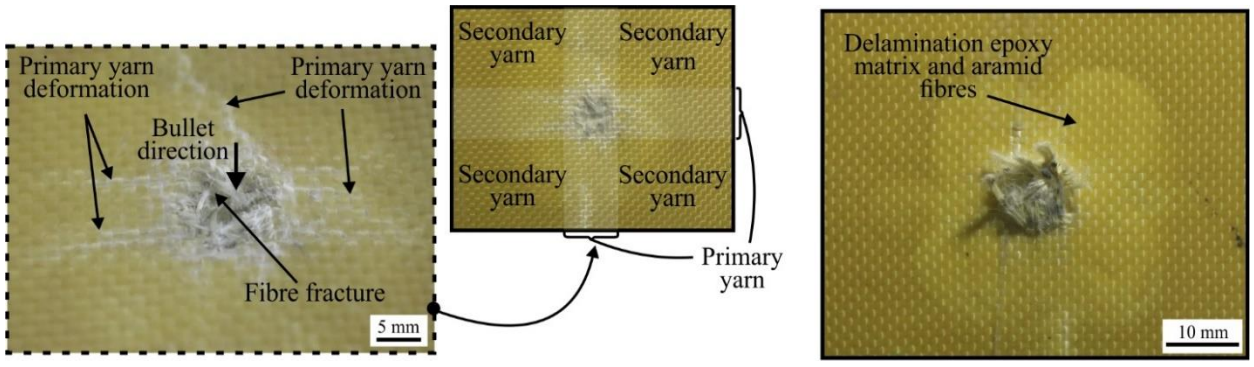

(a) (b)

Figure 10. Ballistic impact in the aramid/epoxy: (a) front face, (b) rear face

Both front and rear sides showed damage to the primary yarn caused by the fiber being unable to withstand the bullet velocity, causing the fiber to break. The impact area also appeared to have delaminated and cracked the epoxy matrix. Fibers that came in direct contact with the bullet triggered a crack in the matrix so that there was a separation in the coating. Delamination that occurs on the front and back sides is one of the main mechanisms of energy absorption. Research has been done by Randjbaran et al., which says that if the area of impact damage is wider, then the amount of ballistic energy absorbed will be higher [33]. The distribution and concentration of stresses on the aramid/epoxy front

view are shown in Figure 11. This can be seen in Figure 11 from the simulation, where the behavior of aramid fabrics under ballistic impact shows that the momentum of the bullet was transferred to the primary yarn (local fabric), while the fabric outside the impact zone (secondary yarn) remained unaffected. These bullet momentum transfers are the same as those reported in previous studies [48-50].

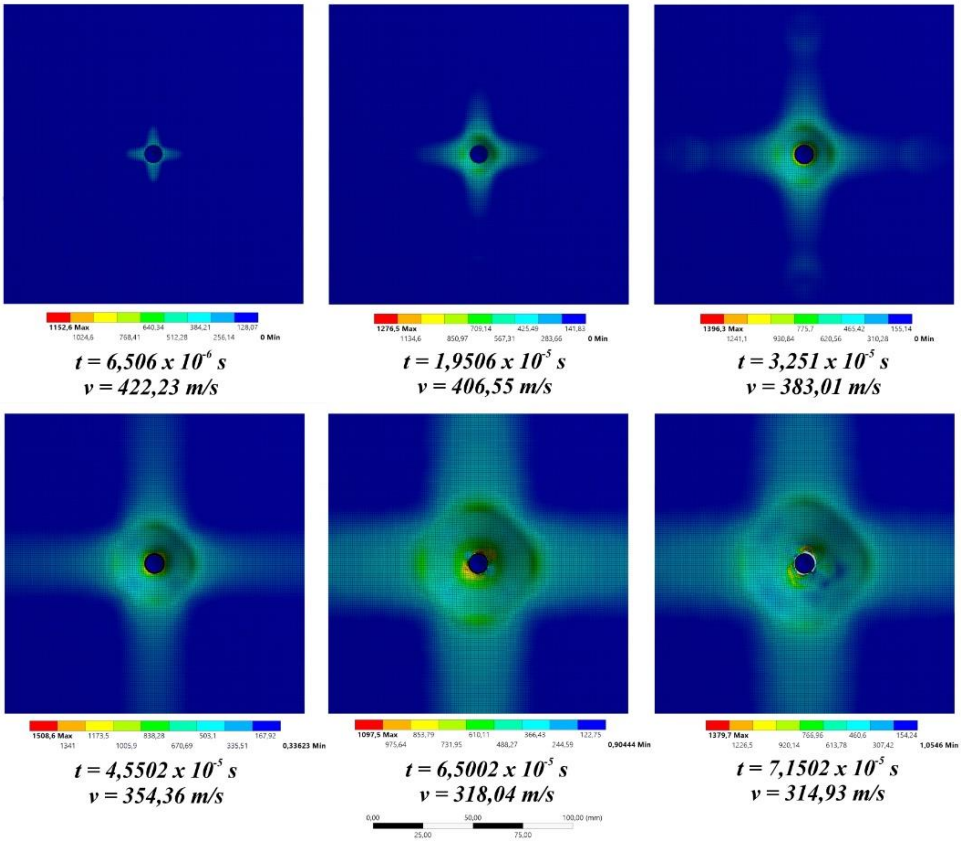

Figure 11. Stress distribution on the fabric aramid/epoxy (front view)

3.2.2 FMLs

Figure 12 depicts the macroscopic features of FMLs following a ballistic impact. The bullet penetration caused a perforation in both the initial aluminum plate layer and the second aramid/epoxy layer, while the last layer deformed into a bulge. FMLs also experienced failure due to delamination, which is the separation between the aluminum plates and the aramid/epoxy. This delamination occurred because the bullet's impact on each layer caused stretching in the areas directly contacted by the bullet, leading to overlapping layers. Two primary energy absorption processes accompany delamination: membrane stretching, which involves plastic deformation, and the failure of translaminar tensile forces. The distribution and concentration of stresses on the FMLs are depicted in Figure 13.

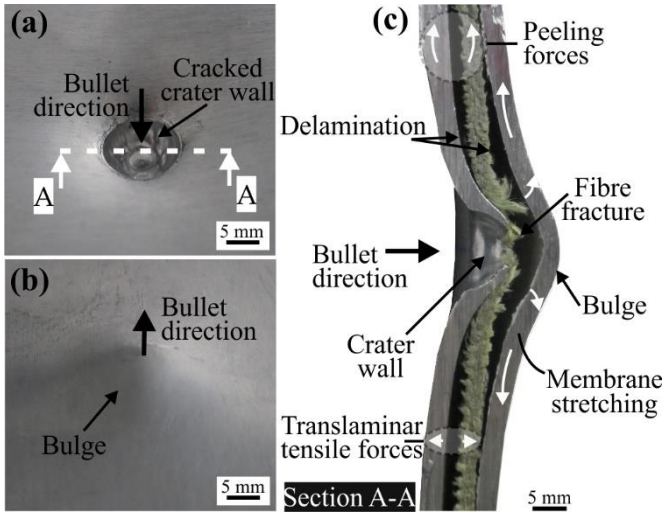

Figure 12. Ballistic impact in the FMLs

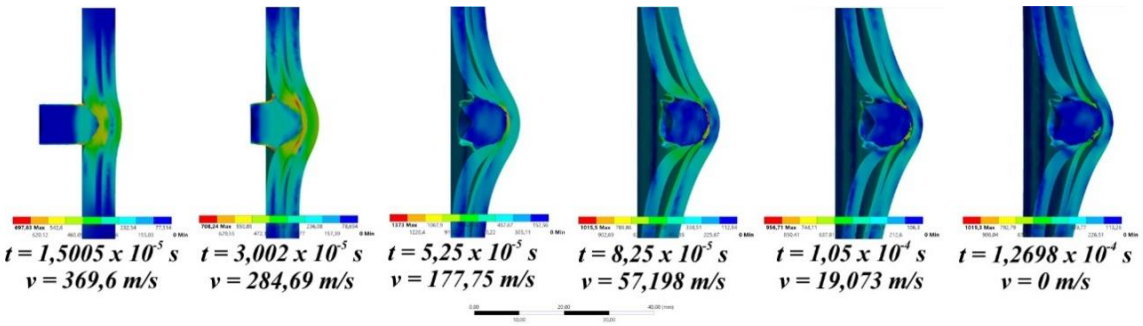

Figure 13. Impact process of the bullet on FML configuration (equivalent stress-von misses)

The bullet tip continued to penetrate the first layer of the aluminum plate while the bullet jacket started to deform and disintegrate at 3.002 x 10-5 seconds. The second layer, which was aramid/epoxy, and the third layer (back plate) were also pushed because of the properties of the ductile materials, resulting in plastic deformation. Penetration on the target stopped after the bullet perforated the first layer (aluminum plate) and the second layer (aramid/epoxy) at 1.2698 x 10-4 seconds.

3.2.3 FMLs with 3 mm holes

Figure 14 shows a comparison of three bullet penetration positions on FMLs with 3 mm holes. The ballistic impact with the center penetration position (FML 3A) and between the ligaments (FML 3C) shows similarity. The bullets are attached to the target, and the formation of petals is found in the area around the hole on the front side of the aluminum plate. The bullet also changed direction so that the bulge on the back side was not top-bottom symmetrical of the bullet coordinate point. The penetration position in the middle of the square center pattern (FML 3B) provided better ballistic resistance, with the bulge formed on the back side looking smoother. One failure due to the ballistic effect in this case was the occurrence of delamination between layers. Delamination that occurred at the center of the penetration position of the hole and between the ligaments of the hole was greater than the center position of the center square pattern, causing the bulge on the back side to also increase. Bonds that are easily separated cause reduced ballistic endurance because plastic deformation is easily formed due to the weak tensile bond between layers [51-52]. The distribution and concentration of stresses in the 3 mm hole FMLs with three bullet penetration positions are shown in Figure 15.

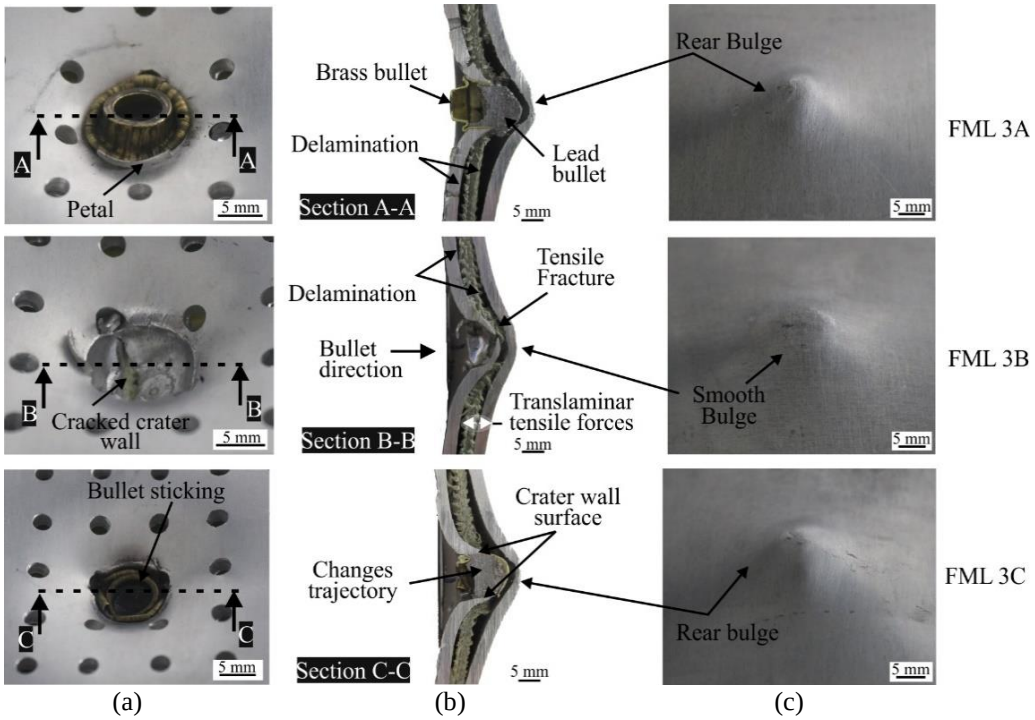

(a) (b) (c)

Figure 14. Ballistic impact in the FMLs with 3 mm holes: (a) front face in the front plate, (b) cross-section, (c) rear face in the back plate

The center penetration position of the hole (Figure 15(a)) caused the bullet to directly perforate the second layer (aramid/epoxy), which experienced a maximum stress of 1015.5 MPa. After the bullet core perforated the target hole, the bullets deviated from its initial trajectory. Plates with holes induce flexural strength in bullets and change the direction of the bullet at 8.05 x 10-5 seconds. Meanwhile, the edges of the bullets were eroded. The initial bullet penetration positions of the middle of the square center pattern and between the ligaments (Figure 15(b)) and (Figure 15(c)) showed similarity,

causing a direct stress distribution to be distributed throughout the FMLs layer. Results demonstrate that the bullet is slowed by a penetration position in the middle of the hole's center square pattern after passing through the first layer (aluminum plate) and the second layer (aramid/epoxy) at 1.2927 x 10^{-4} seconds.

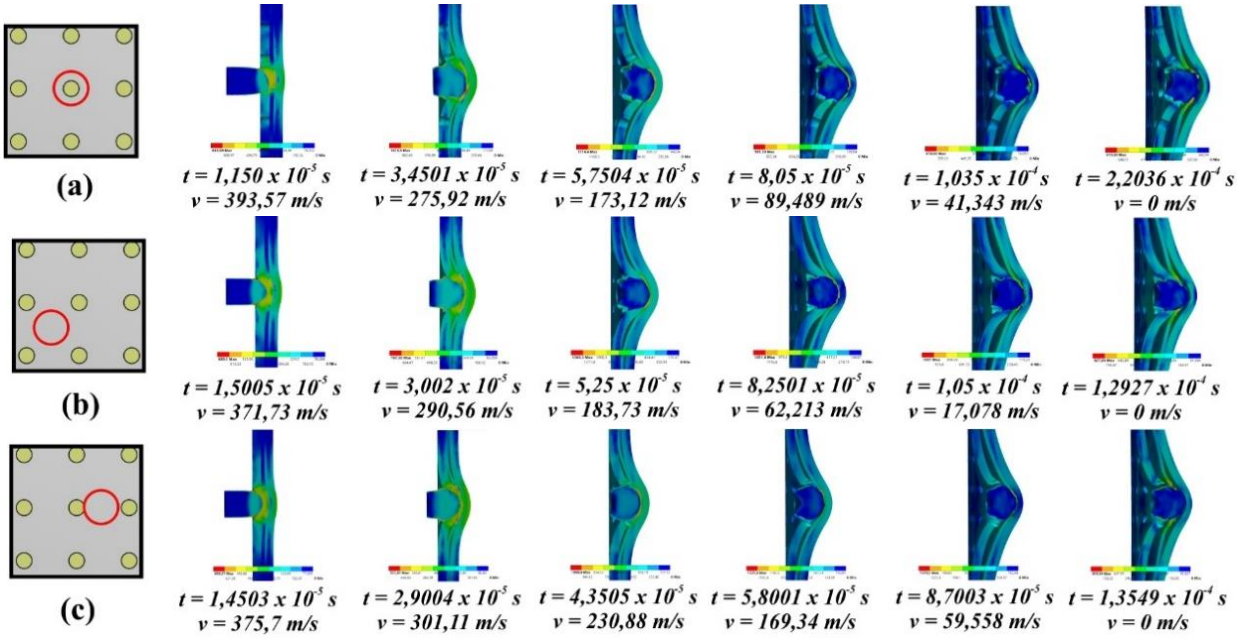

Figure 15. Equivalent von Mises stress on FML with 3 mm hole: (a) center hole, (b) the middle of the square center pattern, (c) between ligament hole

3.2.4 FMLs with 5 mm holes

Figure 16 shows the macroscopic character of three bullet penetration positions in FMLs with 5 mm holes. The center penetration position of the hole (FML 5A) caused the bullet to penetrate and form a fracture on the backside. The fracture at the center penetration position looked like curves and cracks due to collisions. The middle of the square center pattern and between the ligaments (FML 5B and FML 5C) penetrations caused the bullet to stop at the target producing a bulge on the backside. FML failure with 5 mm holes from the three penetration positions was the occurrence of delamination between layers. Very high-velocity bullets caused the first and second layers to be perforated, and the delamination that occurred was not so large compared to when the bullet had its velocity decreased on the back side of the plate (backing plate), which experienced considerable delamination.

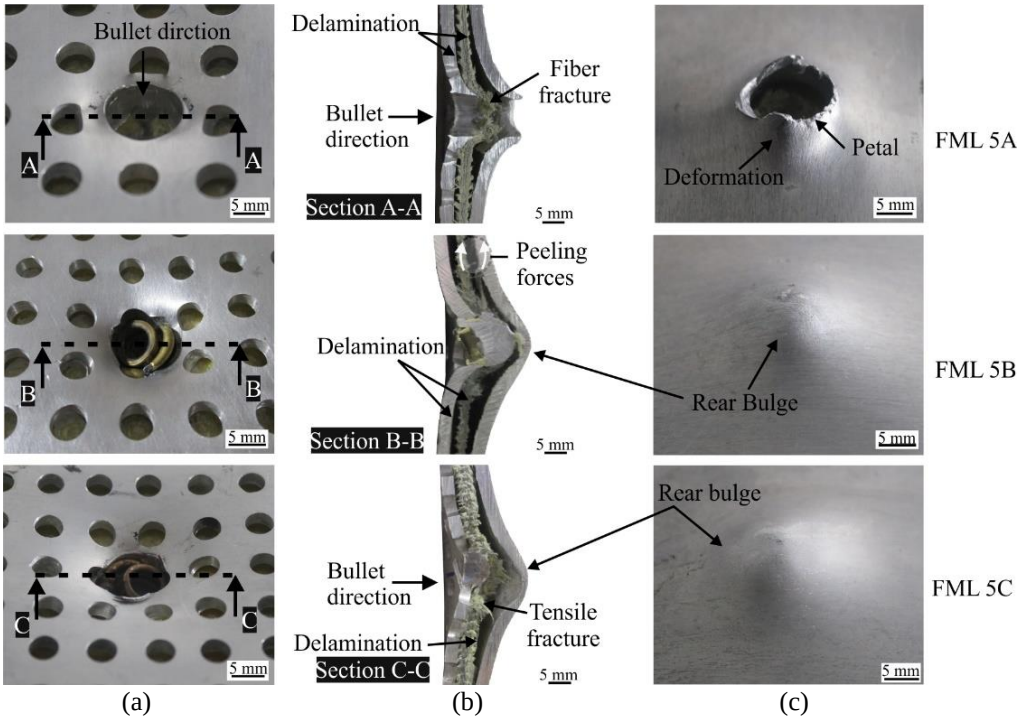

Figure 16. Ballistic impact in the FMLs with 5 mm holes: (a) front face in the front plate, (b) cross-section, (c) rear face in the back plate

The distribution and concentration stresses on FMLs with a 5 mm hole are shown in Figure 17. The center of hole penetration (see Figure 17(a)) caused the hemispherical tip of the bullet to penetrate the second layer directly (aramid/epoxy) and produced a maximum strain of 764.17 MPa. This was because there were no obstacles from the bullet in the first layer, namely the aluminum plate that directly passed through the middle area of the hole. The bullet did not experience a significant decrease in velocity at the beginning of penetration. Figure 17(b) shows a bullet stopping at a target with a faster final velocity at 1.2776 x 10-4 seconds. Meanwhile, the penetration position between ligaments (Figure 17 (c)) shows the final velocity of the bullet at 0 m/s, where the bullet was deformed during penetration at the target, and it seemed the direction of the bullet also changed from its incident trajectory.

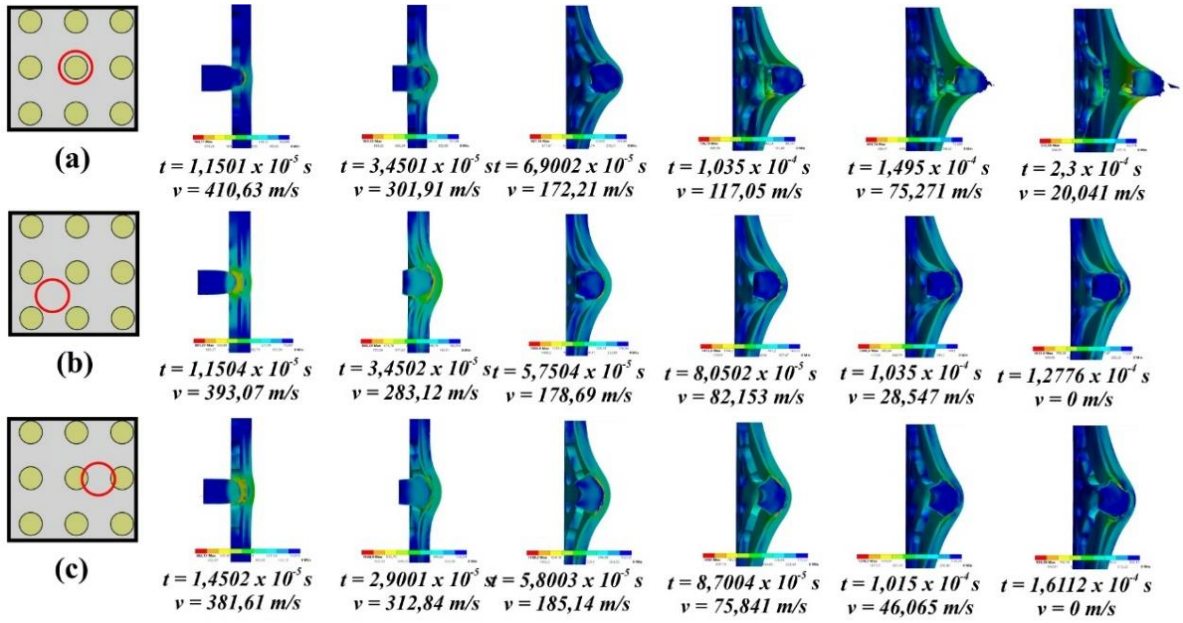

Figure 17. Equivalent von Mises stress on FML with 5 mm hole: (a) center hole, (b) the middle of the square center pattern, (c) between ligament hole

4. DISCUSSION

Figure 18 illustrates the bulge height for all specimen configurations. The high-velocity bullet penetration caused perforation in aluminum plates, aramid/epoxy, and FML 5A specimens. The lowest back-side bulge height, in both experimental and simulation results, was observed in the configuration of FML specimens without holes (FML code). FMLs with a 5 mm hole produced deeper bulges than those with a 3 mm hole due to greater delamination, as shown in Figures 16 and 17. The impact effects vary with the bullet penetration positions in FMLs with holes. Penetration at the center of the square pattern, for both 3 mm and 5 mm hole diameters, produced the smallest bulge, followed by penetration between the ligaments, and finally, penetration at the center of the hole. An exception was noted for the 5 mm diameter hole (FML 5A), which was perforated by the bullet. Figure 19 shows the bullet velocity during penetration at the target.

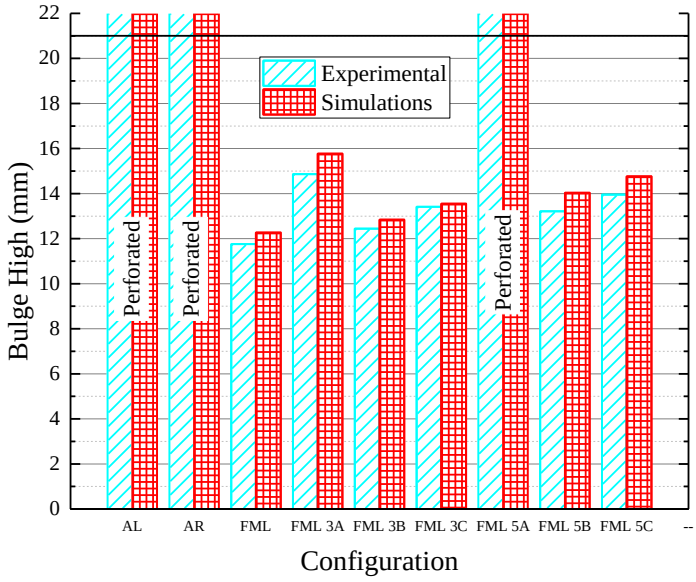

Figure 18. Bulge high after ballistic impact

Table 3. Ballistic test results of FMLs and constituent materials

Material	Bulge High (mm)		Damage
	Experimental	Simulations	
Al	Perforated	Perforated	Plastic deformation, petals
AR	Perforated	Perforated	Perforation, fiber fracture
FML	11,758	12,272	Plastic deformation, crack propagation
FML 3A	14,865	15,774	Plastic deformation, first damage, fiber fracture
FML 3B	12,444	12,839	Plastic deformation, fiber fracture
FML 3C	13,416	13,554	Plastic deformation, fiber fracture
FML 5A	Perforated	Perforated	Large damage, perforation
FML 5B	13,215	14,038	Plastic deformation, fiber fracture
FML 5 C	13,958	14,762	Plastic deformation, fiber fracture

The bullet velocity decreased gradually in all configurations. Both aluminum and aramid/epoxy plate configurations were perforated by bullets, resulting in residual velocities. Aluminum plates had a lower residual velocity compared to aramid/epoxy plates. However, aramid/epoxy showed good ballistic resistance; with only four layers of fiber and a final thickness of 1.12 mm, it achieved a residual velocity similar to that of a 2 mm thick aluminum plate. This is because aramid/epoxy can slow down the bullet and distribute the impact across the vest's cross-section in direct contact with the bullet, leading to multiple deformations.

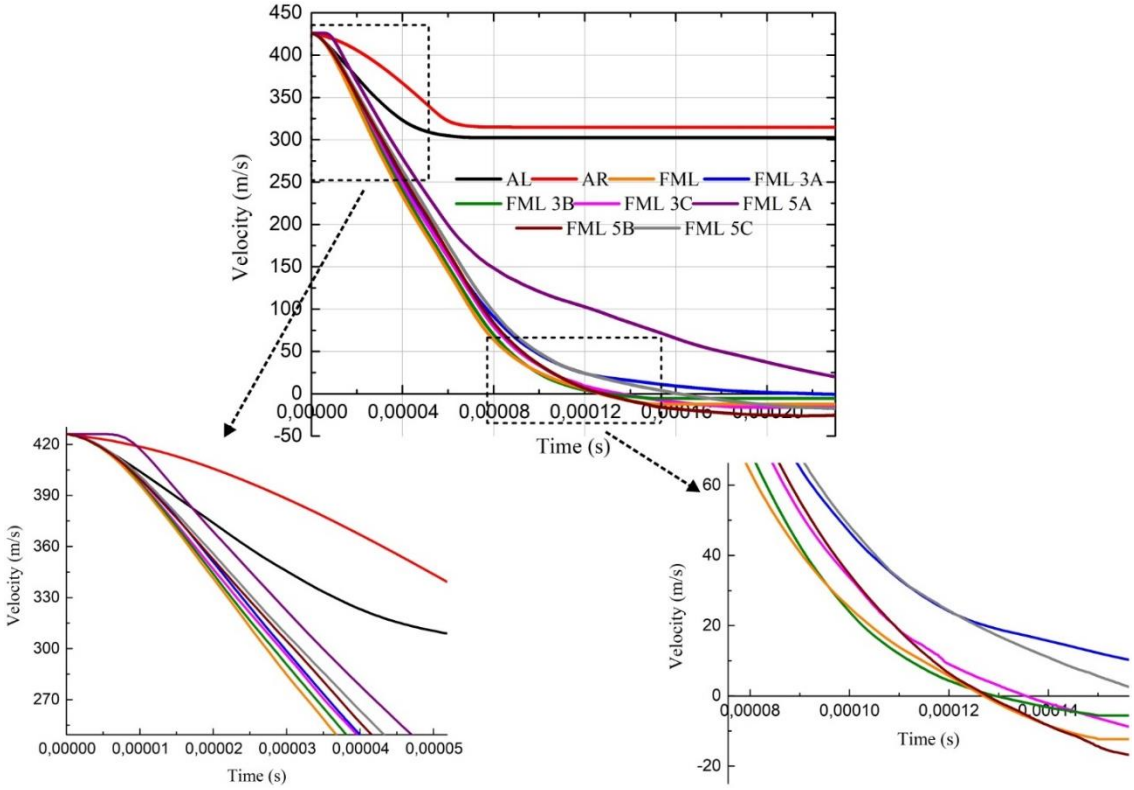

Figure 19. Velocity time histories for different configurations

The FML 5A configuration was similarly perforated by bullets, causing residual velocity to exit the target. In other configurations, the bullet velocity decreased with a final velocity of 0 m/s, which means the bullet was unable to penetrate the target. The direction of the bullet reversed or bounced after penetration on the target to produce a negative value. FML without holes (FML code) was the fastest way to stop the rate of bullets at the initial impact. The penetration of bullets on a plate with a 5 mm hole caused a slower drop in bullet velocity than a 3 mm hole. For holes with diameters of 3 and 5 mm, the position of the bullet penetration in the center of the square pattern hole stopped the bullet rate faster, followed by the penetration position between the ligaments and the center of the hole. Except for the 5 mm diameter hole, which perforated the center of the hole (FML 5C), causing the bullet rate to be constant at the initial impact, this was due to the absence of resistance from the bullet when the penetration happened right in the center of the hole in the first layer (aluminum plate).

The FML 3A configuration caused the bullet velocity to stop at a final speed of 0 m/s, but it took some time. A similar effect was observed in FML 5C, where the bullet velocity slowed gradually at the end of the impact. FMLs without holes

and 3 mm hole FMLs with a penetration position in the center of a square pattern (FML 3B) both stopped the bullet at a final velocity of 0 m/s. FMLs without holes initially reduced the bullet velocity faster, reaching 0 m/s at 1.05 x 10^{-4} seconds. FML 3B appeared to stop the bullet velocity more quickly, with the hole allowing a reduction in velocity at the end of the impact when it perforated the second layer (aramid/epoxy). This is in accordance with previous research reports, which state that monolithic plates with holes have the effect of changing bullet trajectory and decreasing bullet velocity [8]. Figure 20 shows the fracture surface morphology after ballistic impact using scanning electron microscopy (SEM).

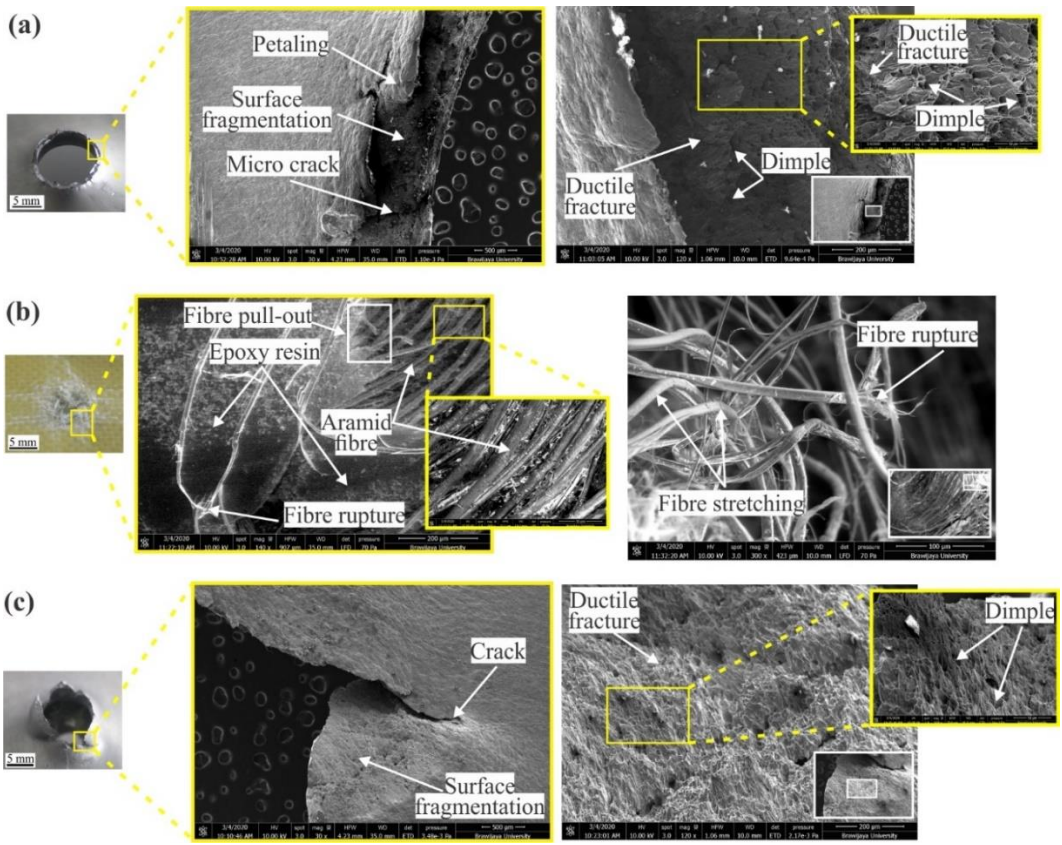

Figure 20. SEM pictures of the fracture surface after ballistic impact: (a) aluminum, (b) aramid/epoxy, (c) FML 5A

The surface appears crushed due to the impact of high-velocity bullets, resulting in a "petaling" effect on the opposite side of the bullet from where it was fired. As the bullet impacts and perforates the target, a shock wave propagates radially outward, causing circular and radial cracks in the plate in front of the bullet. This leads to the petaling effect. SEM results indicate that the predominant failure is ductile fracture, as seen in Figure 20(a), where dimple faults cover almost all sections of the destroyed surface. Figure 20(b) shows the damage area of the aramid/epoxy composite caused by bullet penetration. Near the bullet impact zone, fiber pull-out failure is observed, where aramid fibers are pulled out of the matrix and cracked due to shear forces. However, some parts of the matrix appear to be attached to the fiber at some point. This shows a perfect bond in the interface of the fiber and the matrix. The SEM results on the fracture of the FMLs surface with a 5 mm hole penetrating the center of the hole can be seen in Figure 20(c). The fracture morphology that occurs is a ductile fracture marked by a dominant dimple fault on the entire surface. Dimple fractures are seen as coarser compared to monolithic aluminum plates. This is because the bullet velocity had decreased when penetration in each layer of the target FMLs with the hole, so the remaining bullet velocity at the target also decreased significantly. This is different from the monolithic aluminum plate, which has only experienced a slight decrease in velocity so that the dimple fracture is formed more smoothly.

5. CONCLUSIONS

a) The results from experimental and simulation ballistic impact tests are very similar, showing a 95.63% similarity and a 4.37% error margin.

b) FMLs can withstand bullets by allowing penetration through the first aluminum layer and the second aramid/epoxy layer while the last layer deforms into a bulge. The first layer fails with petaling and dimple fractures, while the second layer shows fiber fractures. Numerical experiments and simulations indicate that a 5 mm diameter hole at the penetration point deepens the rear side bulge, except when the bullet penetrates through the center. Center penetration results in the smallest bulge formation and a quicker reduction in bullet velocity

c) The high-velocity bullet impact causes significant surface crushing and petaling on the target. SEM analysis reveals that the primary failure mode is a ductile fracture characterized by dimple formation. The aramid/epoxy composite

shows fiber pull-out and shear-induced cracks near the impact area, indicating a strong fiber-matrix bond. FML surfaces exhibit coarser dimples due to reduced bullet velocity through each layer, contrasting with smoother dimples in monolithic aluminum plates due to a smaller velocity decrease.

REFERENCES

[1] T. Nieberle, S.R. Kumar, A. Patnaik and C. Goswami "Composite materials for armour application," *Advances in Engineering Design: Select Proceedings of ICOIED 2020*, pp. 239–248. 2021.

[2] U. Mawkhlieng, A. Majumdar and A Laha, "A review of fibrous materials for soft body armour applications," *RSC Advances*, vol. 10, no. 2, pp. 1066–1086, 2020.

[3] F. de Oliveira Braga, T.L. Milanezi, S.N. Monteiro, L.H.L. Louro, A.V. Gomes, and É.P. Lima Jr, "Ballistic comparison between epoxy-ramie and epoxy-aramid composites in Multilayered Armor Systems," *Journal Of Materials Research and Technology*, vol. 7, no. 4, pp. 541–549, 2018.

[4] Office of Law Enforcement Standards of the National Institute of Standards and Technology, U.S. Department of Justice, "Ballistic Resistance of Body Armor NIJ Standard-0101.06," pp. 1-89, 2008.

[5] A. Bhatnagar, Lightweight ballistic composites: Military and law-enforcement applications. Woodhead Publishing, 2016.

[6] S. Vignesh, R. Surendran, T. Sekar and B. Rajeswari, "Ballistic impact analysis of graphene nanosheets reinforced kevlar-29," *Materials Today: Proceedings*, vol. 45, pp. 788–793, 2021.

[7] C.H. Shih, J.L. You, Y.L. Lee, A.Y. Cheng, C.P. Chang, Y.M. Liu et al., "Design and ballistic performance of hybrid plates manufactured from aramid composites for developing multilayered armor systems," *Polymers*, vol. 14, no. 22, pp. 5026, 2022.

[8] A. Mubashar, E. Uddin, S. Anwar, N. Arif, S. Waheed Ul Haq, and M.A.K. Chowdhury, "Ballistic response of 12.7 mm armour piercing projectile against perforated armour developed from structural steel," *Proceedings of the Institution of Mechanical Engineers, Part L: Journal of Materials: Design and Applications*, vol. 233, no. 10, pp. 1993-2005, 2018.

[9] J. Deng, J. Zhang, X. Zhang and K. Bao "Investigation on bullet proof mechanism of yag transparent ceramic composite targets," *Transactions of Beijing Institute of Technology*, vol. 42, no. 6, pp. 620–628, 2022.

[10] M. Wu, C. Zhi, L. Tu, Y. Wang, Y. Dai, L. Yu et al. "Cotton-containing printing wires based on the two-dimensional braiding method for three-dimensional printing of clothing," T*extile Research Journal*, vol. 92, no. 9–10, pp. 1384–1393, 2022.

[11] V. Mahesh, S. Joladarashi and S.M. Kulkarni "A comprehensive review on material selection for polymer matrix composites subjected to impact load," *Defence Technology*, vol. 17, no. 1, pp. 257–277, 2021.

[12] F.S. Luz, F.C. Garcia Filho, M.S. Oliveira and L.F.C. Nascimento "Composites with natural fibers and conventional materials applied in a hard armor: A comparison," *Polymers*, vol. 12, no. 9, pp. 1920, 2020.

[13] Z. Ding, H. Wang, J. Luo and N. Li "A review on forming technologies of fibre metal laminates," *International Journal of Lightweight Materials and Manufacture*, vol. 4, no. 1, pp. 110–126, 2021.

[14] W. Zhang and J. Xu "Advanced lightweight materials for Automobiles: A review," *Materials & Design*, vol. 221, p. 110994, 2022.

[15] Y. Chen, Y. Wang and H. Wang, "Research progress on interlaminar failure behavior of fiber metal laminates," *Advances in Polymer Technology*, vol. 2020, no. 1, pp. 3097839, 2020.

[16] M. Soroush, K.M. Fard, and M. Shahravi, "Finite element simulation of interlaminar and intralaminar damage in laminated composite plates subjected to impact," *Latin American Journal of Solids and Structures*, vol. 15, no. 6, p. e90, 2018.

[17] S. Chandrabakty, I. Renreng, Z. Djafar and H. Arsyad "Experimental study and investigation of thrust force and delamination damage of drilled ramie woven reinforced composites," *International Journal of Automotive and Mechanical Engineering*, vol. 17, no. 1, pp. 7618–7628, 2020.

[18] G.G. Braga, G. Giusti, J.C. dos Santos, D.A.L. Silva, A.L. Christoforo, T.H. Panzera et al. "Life cycle assessment of fibre metal laminates: An ecodesign approach," *Composites Part C: Open Access*, vol. 13, pp. 100435, 2024.

[19] K. Jin, K. Chen, X. Luo and J. Tao "Fatigue crack growth and delamination mechanisms of Ti/CFRP fibre metal laminates at high temperatures," *Fatigue & Fracture of Engineering Materials & Structures*, vol. 43, no. 6, pp. 1115–1125, 2020.

[20] F. Czerwinski, "Current trends in automotive lightweighting strategies and materials," *Materials*, vol. 14, no. 21, p. 6631, 2021.

[21] J.G. Carrillo, N.G. Gonzalez-Canche, E.A. Flores-Johnson, and P. Cortes, "Low velocity impact response of fibre metal laminates based on aramid fibre reinforced polypropylene," *Composite Structures*, vol. 220, pp. 708–716, 2019.

[22] D.-W. Lee, B.-J. Park, S.-Y. Park, C.-H. Choi, and J.-I. Song, "Fabrication of high-stiffness fiber-metal laminates and study of their behavior under low-velocity impact loadings," *Composite Structures*, vol. 189, pp. 61–69, 2018.

[23] L. Li, Q.C. Zhang and T.J. Lu "Ballistic penetration of deforming metallic plates: Experimental and numerical investigation," *International Journal of Impact Engineering*, vol. 170, pp. 104359, 2022.

[24] M.H. Mosa and M.N. Hamza "Influence of selection materials and construction techniques on the ballistic performance of armors: A review," In *AIP Conference Proceedings*, vol. 2404, no. 1, 2021.

[25] M.G. Stewart and M.D. Netherton, "Statistical variability and fragility assessment of ballistic perforation of steel plates for 7.62 mm AP ammunition." *Defence Technology*, vol. 16, no. 3, pp. 503–513, 2020.

[26] R. Scazzosi, M. Giglio and A. Manes "Experimental and numerical investigation on the perforation resistance of double-layered metal shield under high-velocity impact of armor-piercing projectiles," *Materials*, vol. 14, no. 3, p. 626, 2021.

[27] K. Senthil and M.A. Iqbal "Prediction of superior target layer configuration of armour steel, mild steel and aluminium 7075-T651 alloy against 7.62 AP projectile," *Structures,* vol. 29, pp. 2106–2119, 2021.

[28] A. Rashed, M. Yazdani, A.A. Babaluo, and P.H. Parvin, "Investigation on high-velocity impact performance of multi-layered alumina ceramic armors with polymeric interlayers," *Journal of Composite Materials*, vol. 50, no. 25, pp. 3561–3576, 2016.

[29] N. Nayak, A. Banerjee, and T.R. Panda, "Numerical study on the ballistic impact response of aramid fabric-epoxy laminated composites by armor piercing projectile," *Procedia Engineering*, vol. 173, pp. 230–237, 2017.

[30] Choudhary, S., Singh, P. K., Khare, S., Kumar, K., Mahajan, P., and Verma, R. K. "Ballistic impact behaviour of newly developed armour grade steel: An experimental and numerical study." *International Journal of Impact Engineering*, vol. 140, pp. 103557, 2020.

[31] Jo, M. C., Kim, S., Suh, D. W., Hong, S. S., Kim, H. K., Sohn, S. S., and Lee, S. "Effect of tempering conditions on adiabatic shear banding during dynamic compression and ballistic impact tests of ultra-high-strength armor steel." *Materials Science and Engineering: A*, vol. 792, pp. 139818, 2020.

[32] Asemani, S. S., Liaghat, G., Ahmadi, H., Anani, Y., Khodadadi, A., and Charandabi, S. C. "The experimental and numerical analysis of the ballistic performance of elastomer matrix Kevlar composites." *Polymer Testing*, vol. 102, pp. 107311, 2021.

[33] Fadly, M. S., Bakri, B., Anwar, K., and Chandrabakty, S. "Evaluation of Projectile Penetration Position on Perforated Plate on Ballistic Resistance of Composite Sandwich Panels." In *IOP Conference Series: Earth and Environmental Science*, vol. 1157, pp. 12033, 2023.

[34] M. A. Abtew, F. Boussu, P. Bruniaux, C. Loghin, and I. Cristian, "Ballistic impact mechanisms-A review on textiles and fibre-reinforced composites impact responses," *Compos. Struct.*, vol. 223, p. 110966, 2019.

[35] B. Bakri, M.S. Fadly, K. Anwar and S. Chandrabakty, "Numerical research on the impacts of composite panel ballistic using perforated plate for combat vehicle," In *4th International Seminar on Science and Technology (ISST 2022)*, pp. 15–25, 2023.

[36] R.S. Sikarwar, R. Velmurugan, and N.K. Gupta, "Ballistic performance of Kevlar/epoxy composite laminates," *Proceedings of the Indian National Science Academy*, vol. 79, no. 4, p. 789, 2015.

[37] M.S. Fadly, A. Purnowidodo, P.H. Setyarini, B. Bakri and S. Chandrabakty "Perforation and penetration of fiber metal laminates target by hemispherical projectile," *International Journal of Mechanical Engineering Technologies and Applications*, vol. 4, no. 2, pp. 190–197, 2023.

[38] I.A. Saleem, P.S. Ahmed and M.S. Abed "Experimental and numerical investigation of Kevlar and UHMWPE multi-layered armors against ballistic impact," *Materials Today: Proceedings*, vol. 56, pp. 2516–2524, 2022.

[39] Y. Heng, X. Qi, L. Xu, Y. Yan and Q. Ni "Development of high-strength carbon fiber/thermoplastic epoxy resin composites and it's recyclability," *Polymer Composites*, vol. 45, no. 10, pp. 8710–8720, 2024.

[40] J. Chen, Y. Zhu, Q. Ni, Y. Fu and X. Fu, "Surface modification and characterization of aramid fibers with hybrid coating," *Applied Surface Science*, vol. 321, pp. 103–108, 2014.

[41] R.S. Talikoti and S.B. Kandekar, "Strength and durability study of concrete structures using aramid-fiber-reinforced polymer," *Fibers*, vol. 7, no. 2, p. 11, 2019.

[42] Y. Wang, X. Zeng, H. Chen, X. Yang, F. Wang and L. Zeng, "Modified Johnson-Cook constitutive model of metallic materials under a wide range of temperatures and strain rates," *Results in Physics*, vol. 27, p. 104498, 2021

[43] T. Hanaoka, Y. Arao, Y. Kayaki, S. Kuwata and M. Kubouchi "Analysis of nitric acid decomposition of epoxy resin network structures for chemical recycling," *Polymer Degradation and Stability*, vol. 186, p, 109537, 2021

[44] Y. Zhou, G. Li, Q. Fan, Y. Wang, H. Zheng, L. Tan et al., "Study on protection mechanism of 30CrMnMo-UHMWPE composite armor," *Materials*, vol. 10, no. 4, p. 405, 2017.

[45] T. Liu, X. Zhang, N. He, and G. Jia, "Numerical material model for composite laminates in high-velocity impact simulation," *Latin American Journal of Solids and Structures*, vol. 14, no. 11, pp. 1912–1931, 2017.

[46] H. Sinan Üstün, A. Kaan Toksoy and M. Tanoğlu, "Investigation of hybridization effect on ballistic performance of multi-layered fiber reinforced composite structures." *Journal of Composite Materials*, vol. 56, no. 15, pp. 2411–2431, 2022.

[47] A. Shi, X. Hong, H. Han, K. Xia, X. Fan, C. Qin et al., "Research on ballistic protection characteristics of perforated plates made of different steel materials for 12.7 mm penetrator projectile," In *Journal of Physics: Conference Series*, vol. 2808, p. 12007, 2024.

[48] C. Stephen, B. Shivamurthy, R. Selvam, S.R. Behara, A.H.I. Mourad and S. Kannan, "Design and finite element study of Kevlar based combat helmet for protection against high-velocity impacts," *Materials Today: Proceedings*, vol. 56, pp. 3636–3641, 2022.

[49] M.A. Iqbal, K. Senthil, P. Bhargava, and N.K. Gupta, "The characterization and ballistic evaluation of mild steel," *International Journal of Impact Engineering*, vol. 78, pp. 98–113, 2015.

[50] V. Mahesh, S. Joladarashi and S.M. Kulkarni "Comparative study on ballistic impact response of neat fabric, compliant, hybrid compliant and stiff composite," *Thin-Walled Structures*, vol. 165, p. 107986, 2021.

[51] P. Kędzierski, A. Popławski, R. Gieleta, A. Morka, and G. Sławiński, "Experimental and numerical investigation of fabric impact behavior," *Composites Part B: Engineering*, vol. 69, pp. 452–459, 2015.

[52] B. Bakri, K. Anwar, M.S. Fadly and K. Wahyudi "Investigation of ballistic performance on metal-coir fiber composite laminate with variation of fiber volume fraction: Experimental and simulation," In *IOP Conference Series: Earth and Environmental Science*, vol. 1355, pp. 12010, 2024.